ELSEVIER

Biophysical Chemistry 113 (2005) 233–244

Biophysical Chemistry

www.elsevier.com/locate/bpc

Structure and properties of phospholipid–peptide monolayers containing monomeric SP-$B_{1–25}$ II. Peptide conformation by infrared spectroscopy

Saratchandra Shanmukh[a], Nilanjana Biswas[a], Alan J. Waring[b,c], Frans J. Walther[c], Zhendong Wang[d], Y. Chang[d], Robert H. Notter[d], Richard A. Dluhy[a,*]

[a]*Department of Chemistry, University of Georgia, Athens, GA 30602-2556, United States*
[b]*Department of Medicine, Division of Infectious Diseases, Center for the Health Sciences, UCLA, 10833 Le Conte Avenue, Los Angeles, CA 90095, United States*
[c]*Department of Pediatrics, Research and Education Institute at Harbor-UCLA Medical Center, 1124 West Carson Street, Building F-5 South, Torrance, CA 90502, United States*
[d]*University of Rochester, Department of Pediatrics, Box 850, Neonatology, 601 Elmwood Avenue, Rochester, NY 14642, United States*

Received 20 July 2004; received in revised form 15 September 2004; accepted 15 September 2004
Available online 18 October 2004

Abstract

The conformation and orientation of synthetic monomeric human sequence SP-$B_{1–25}$ (mSP-$B_{1–25}$) was studied in films with phospholipids at the air–water (A/W) interface by polarization modulation infrared reflectance absorption spectroscopy (PM-IRRAS). Modified two-dimensional infrared (2D IR) correlation analysis was applied to PM-IRRAS spectra to define changes in the secondary structure and rates of reorientation of mSP-$B_{1–25}$ in the monolayer during compression. PM-IRRAS spectra and 2D IR correlation analysis showed that, in pure films, mSP-$B_{1–25}$ had a major α-helical conformation plus regions of β-sheet structure. These α-helical regions reoriented later during film compression than β structural regions, and became oriented normal to the A/W interface as surface pressure increased. In mixed films with 4:1 mol:mol acyl chain perdeuterated 1,2-dipalmitoyl-*sn*-glycero-3-phosphocholine/1,2-dioleoyl-*sn*-glycero-3-[phospho-*rac*-(1-glycerol)] (sodium salt) (DPPC-d_{62}:DOPG), the IR spectra of mSP-$B_{1–25}$ showed that a significant, concentration-dependent conformational change occurred when mSP-$B_{1–25}$ was incorporated into a DPPC-d_{62}:DOPG monolayer. At an mSP-$B_{1–25}$ concentration of 10 wt.%, the peptide assumed a predominately β-sheet conformation with no contribution from α-helical structures. At lower, more physiological peptide concentrations, 2D IR correlation analysis showed that the propensity of mSP-$B_{1–25}$ to form α-helical structures was increased. In phospholipid films containing 5 wt.% mSP-$B_{1–25}$, a substantial α-helical peptide structural component was observed, but regions of α and β structure reoriented together rather than independently during compression. In films containing 1 wt.% mSP-$B_{1–25}$, peptide conformation was predominantly α-helical and the helical regions reoriented later during compression than the remaining β structural components. The increased α-helical structure of mSP-$B_{1–25}$ demonstrated here by PM-IRRAS and 2D IR correlation analysis in monolayers of 4:1 DPPC:DOPG containing 1 wt.% (and, to a

Abbreviations: ALI, acute lung injury; ARDS, acute respiratory distress syndrome; A/W, air–water; DPPC, 1,2-dipalmitoyl-*sn*-glycero-3-phosphocholine; DPPC-d_{62}, 1,2-dipalmitoyl-d_{62}-*sn*-glycero-3-phosphocholine; DOPG, 1,2-dioleoyl-*sn*-glycero-3-[phospho-*rac*-(1-glycerol)] (sodium salt); HEPES, *N*-(2-hydroxyethyl)piperizine-*N*′-(2-ethanesulfonic acid); HMP, 4-hydroxymethylphenoxyacetyl-4′-methylbenzyhydrylamine resin; IRRAS, infrared reflection absorbance spectroscopy; PM-IRRAS, polarization–modulation infrared reflectance–absorption spectroscopy; RDS, respiratory distress syndrome; SP-B/C, naturally isolated mixture of hydrophobic surfactant peptides B and C; SP-B, pulmonary surfactant protein B; SP-$B_{1–25}$, synthetic peptide containing first 25 amino acids of the N-terminal of SP-B; SP-C, pulmonary surfactant protein C; TFA, trifluoroacetic acid; 2D IR, two-dimensional infrared correlation analysis; TFE, trifluoroethanol.

* Corresponding author. Tel.: +1 706 542 1950; fax: +1 706 542 9454.
E-mail address: dluhy@chem.uga.edu (R.A. Dluhy).

doi:10.1016/j.bpc.2004.09.009

lesser extent, 5 wt.%) peptide may be relevant for the formation of the intermediate order 'dendritic' surface phase observed in similar surface films by epi-fluorescence.

Keywords: mSP-$B_{1–25}$; Surfactant protein (SP)-B; Polarization–modulation IR spectroscopy; 2D IR correlation analysis; Lung surfactants; Synthetic peptides

1. Introduction

Pulmonary surfactant protein B (SP-B) is a highly active component of endogenous lung surfactant, with an amphipathic molecular structure capable of interacting strongly with both hydrophobic and hydrophilic regions of phospholipids to increase adsorption and overall dynamic surface tension lowering [1–5]. SP-B is also a functionally crucial constituent in clinical exogenous surfactants used to treat diseases of surfactant deficiency or dysfunction such as the neonatal respiratory distress syndrome (RDS), clinical acute lung injury (ALI), and the acute respiratory distress syndrome (ARDS) [5,6]. Because of the functional importance of SP-B in endogenous and exogenous surfactants, its molecular biophysical behavior has been of significant research interest. Although a good deal is now known about the structure and activity of SP-B, its specific interactions and molecular orientations directly in interfacial films with phospholipids are not yet completely defined. The full-length SP-B protein is thought to have at least five to six distinct domains [7–10], including an N-terminal region with a short insertion sequence that can assume an extended β-sheet conformation and is adjacent to a stable amphipathic helix.

One approach to elucidating the contributions to activity of different structural regions of SP-B involves the study of synthetic peptides such as SP-$B_{1–25}$, which incorporates the 25 amino acids in the important N-terminal region of the native protein [11–16]. In a companion study, we have used epifluorescence techniques to investigate the morphology and phase behavior of compressed interfacial films containing human sequence monomeric SP-$B_{1–25}$ (mSP-$B_{1–25}$) plus 4:1 mol:mol 1,2-dipalmitoyl-*sn*-glycero-3-phosphocholine (DPPC)/1,2-dioleoyl-*sn*-glycero-3-[phospho-*rac*-(1-glycerol)] (sodium salt) (DOPG) [17]. The present paper examines the molecular behavior of mSP-$B_{1–25}$ in films with 4:1 acyl chain perdeuterated 1,2-dipalmitoyl-*sn*-glycero-3-phosphocholine (DPPC-d_{62}:DOPG at the air–water (A/W) interface using polarization–modulation IR reflection–absorption spectroscopy (PM-IRRAS). PM-IRRAS has several advantages over conventional polarized IR reflectance spectroscopy for studying molecular properties in films at the A/W interface. These include the ability to discriminate isotropic water and water vapor absorptions, as well as to analyze spectra directly for molecular orientations and conformations in the interfacial film in situ [18].

We have previously used conventional monolayer IR spectroscopy as well as PM-IRRAS to examine the molecular interactions of bovine naturally isolated mixture of hydrophobic surfactant peptides B and C (SP-B/C) in monolayers with synthetic phospholipids at the A/W interface [19,20]. In addition, the conformation of SP-$B_{1–25}$ has been investigated in experimental studies [12,13] and in computer simulations [14,16]. However, there is little or no information on the orientation and conformation of this peptide in interfacial monolayers containing DPPC plus an unsaturated anionic component (DOPG) as occurs in native lung surfactant. The results presented here provide the first direct spectroscopic analyses of the structure and orientation of mSP-$B_{1–25}$ in a phospholipid matrix at the A/W interface. They also complement epi-fluorescence experiments carried out in a companion study on morphological and phase changes in monolayers of 4:1 DPPC:DOPG with 1, 5, and 10 wt.% mSP-$B_{1–25}$ [17].

2. Materials and methods

2.1. Synthetic materials

The synthetic acyl chain perdeuterated phospholipid 1,2-dipalmitoyl-*sn*-glycero-3-phosphocholine (DPPC-d_{62}) as well as 1,2-dioleoyl-*sn*-glycero-3-[phospho-*rac*-(1-glycerol)] (sodium salt) (DOPG) were purchased from Avanti Polar Lipids (Alabaster, AL). These lipids were specified as >99% pure and were used as supplied. High-performance liquid chromatography (HPLC)-grade methanol and chloroform were obtained from J.T. Baker (Phillipsburg, NJ). Ultrapure NaCl was obtained from Fluka. Ultrapure H_2O used for film balance subphases and in all cleaning procedures was obtained from a Barnstead (Dubuque, IA) ROpure/Nanopure reverse osmosis/deionization system, and had a nominal resistivity of 18.3 MΩ cm. Film balance subphases in all experiments were 120 mM NaCl adjusted to pH 7.

2.2. Peptide synthesis and purification

SP-$B_{1–25}$ (NH_2-FPIPLPYCWLCRALIKRIQAMIPKG-COOH) was made by solid-phase peptide synthesis employing *O*-fluorenylmethyl-oxycarbonyl (Fmoc) chemistry. Fmoc amino acids and coupling agents were from AnaSpec (San Jose, CA). Solvents and other reagents used for peptide synthesis and purification were HPLC grade or better (Fisher Scientific, Tustin, CA; Aldrich Chemical, Milwaukee, WI). The peptide was synthesized on a 0.25 mmol scale with an ABI 431A peptide synthesizer configured for FastMoc™ double-coupling cycles [21] utilizing a prederivatized *N*-α-Fmoc-glycine 4-hydroxymethylphenoxyace-

tyl-4′ -methylbenzyhydrylamine resin (HMP; AnaSpec, San Jose, CA). Deprotection and cleavage of the peptide from the resin was carried out using trifluoroacetic acid (TFA)/thioanisol/EDT/phenol/water (10:0.5:0.25:0.5:0.5 by vol.) for 2 h followed by cold precipitation with *t*-butyl ether. The crude product was then purified by preparative reverse phase HPLC with a Vydac C-18 column and a water/acetonitrile linear gradient with 0.1% trifluoroacetic acid as described previously [22]. The molecular weight of the peptide was determined by fast atom bombardment and/or MALDI-TOF mass spectrometry, and purity of>95% was confirmed by analytical HPLC and capillary electrophoresis.

2.3. Preparation of lipid–peptide mixtures

Stock phospholipid solutions of DPPC-d_{62} and DOPG (~1 mg/ml) were prepared in 3:1 $CHCl_3$:MeOH. For the phospholipid–peptide mixtures, the required volume of mSP-$B_{1–25}$ in 1:1 $CHCl_3$:MeOH was evaporated with N_2 for ~30 min to ensure complete solvent evaporation. The dried protein film was then dissolved in a volume of 2,2,2-trifluoroethanol (TFE). An appropriate volume of the DPPC-d_{62}:DOPG stock phospholipid solution was then added to the protein solution in TFE. The resultant phospholipid–protein solution was evaporated for ~45 min with N_2, and left overnight in a vacuum desiccator for complete elimination of solvent. The dried lipid–protein sample was then dissolved in 3:1 $CHCl_3$:MeOH for use in the monolayer IR studies.

2.4. Polarization–modulation IR reflection–absorption spectroscopy (PM-IRRAS)

Spectroscopic measurements of lipid-peptide monolayers at the A/W interface were performed using a Bruker Instruments (Billerica, MA) Equinox 55 Fourier transform infrared spectrometer optically interfaced to a variable angle external reflection accessory (Bruker model XA511-A). The external reflection accessory was equipped with a custom-designed Langmuir trough (Riegler and Kirstein, Berlin, Germany) containing a microbalance Wilhelmy sensor for surface pressure readings. Films were spread dropwise from a $CHCl_3$:MeOH solution at the A/W interface, and surface spectra were acquired at 22±0.3 °C. PM-IRRAS measurements were performed using previously described protocols adapted for our experimental design [23].

The IR beam from the interferometer was directed through its external beam port and steered using mirrors into the excitation arm of the reflectance accessory. This IR beam was singly modulated at frequencies $f=2V\tilde{\nu}$, where V is the scan speed of the interferometer and $\tilde{\nu}$ is the wavenumber of the IR radiation, resulting in a spectral bandwidth of approximately 0.4–6.5 kHz. The excitation arm of the external reflection accessory was rotated using computer-driven stepper motors to achieve an angle of incidence of 74°. Before reflection from the A/W interface, a wire grid polarizer (IGP225, Molectron Detector, Portland, OR) passed *p*-polarized light through a ZnSe photoelastic modulator (PEM-90, Hinds Instruments, Hillsboro, OR) operating at its resonance frequency f_m of 50 kHz. The application of a sinusoidal input voltage to the PEM crystal induced a linear modulation of the IR beam between *p*- and *s*-polarization states at a 2 f_m frequency of 100 kHz, resulting in a second, high-frequency modulation of the IR radiation. After reflection from the A/W interface, the doubly modulated IR radiation was collected by an *f*/1 ZnSe lens and focused onto the 1-mm^2 sensing chip of a liquid N_2-cooled photovoltaic HgCdTe detector (KMPV11, Kolmar Technologies, Newburyport, MA).

Because the spectral frequencies from the interferometer were more than an order of magnitude removed from the modulation frequencies added by the PEM, the signal from the HgCdTe detector preamplifier was separated into sum (I_{dc}—resulting from the IR spectrometer) and difference (I_{ac}—resulting from PEM modulation) components using dual-channel electronics with lock-in detection, as previously described [18]. The I_{ac} difference signal was demodulated at 2 f_m with a digital lock-in amplifier (Stanford Research Systems, Model SR830) using a 100 μs time constant. The I_{ac} difference signal from the output of the lock-in, as well as the I_{dc} sum signal, was filtered using low-pass filters; electronic filtering was achieved using dual-channel electronics (Stanford Research System, Model SR650). At the output of the electronic filters, both I_{ac} and I_{dc} signals were combined using a multiplexer and were sent to the 16-bit ADC of the Bruker IR spectrometer. The combined signal was deconstructed and Fourier-transformed using spectrometer software. The ratio of the resulting I_{ac} and I_{dc} single-beam spectra provides the PM-IRRAS signal S.

$$S = \frac{I_{ac}}{I_{dc}} = C\frac{J_2(\phi)(R_p - R_s)}{(R_p + R_s) + J_0(\phi)(R_p - R_s)} \quad (1)$$

In this equation, C is a constant that is the ratio of the slightly different electronic amplification of the two signal channels, and $J_n(\phi_0)$ is the nth-order Bessel function of maximum dephasing ϕ_0 introduced by the PEM (set here to introduce maximum dephasing, $\phi_0=\pi$, at 1750 cm^{-1}). PM-IRRAS spectra were normalized as difference spectra, with ΔS defined as the difference in signal intensity between the film-covered surface (S) and the bare water surface (S_0):

$$\Delta S = \frac{S - S_0}{S_0} \quad (2)$$

Spectra were recorded at a resolution of 4 cm^{-1} using a scan speed/sampling frequency of 13 kHz. The total acquisition time for each spectrum was 16 min, resulting in 1500 interferograms per spectrum.

2.5. Calculation of exponential 2D IR correlations—kv correlation analysis

A *kv* correlation analysis is a mathematical cross correlation performed between a set of *N* spectra undergoing some dynamic intensity variation against a set of decreasing exponential functions that are varying in their rate constants [24]. As such, it is a model-dependent two-dimensional infrared correlation analysis (2D IR) correlation method analogous to the *βv* correlation analysis method that we have previously described and applied to biophysical monolayer systems [19,25]. The *kv* correlation analysis used here is mathematically described as shown in Eq. (3). The asynchronous correlation intensity Ψ at some point (v, k) represents the correlation of the measured IR spectral intensity $y(v, n_j)$ with the mathematical function $\exp(-kt+R)$. In Eq. (3), y is the IR intensity; v is the frequency or wavenumber; n_j is the number of the spectrum in the ordered sequence where the first spectrum number is zero; k is the rate constant of the exponential curve; N is the total number of spectra used in the calculation; R is a constant matrix, and M_{jk} is the Hilbert-Noda transform which is defined in Eq. (4).

$$\Psi(v,k) = \frac{1}{N-1}\sum_{j=0}^{N-1} y(v,n_j)\sum_{k=0}^{N-1} M_{jk}\exp(-kt+R) \quad (3)$$

$$M_{jk} = \begin{cases} 0 & \text{if } j = k \\ 1/\pi(k-j) & \text{otherwise} \end{cases} \quad (4)$$

Only the asynchronous correlation algorithm is used in the *kv* correlation analyses presented in this study, since asynchronous 2D IR correlations are more sensitive to differences in the form of the signal variation than are synchronous correlations [26]. The computational algorithm for the *kv* correlation analysis uses the most recent mathematical formalism in which a Hilbert-Noda transform is used for calculating the asynchronous spectrum rather than the more computationally cumbersome Fourier transform [27].

Two-dimensional *kv* correlation analyses were performed on monolayer PM-IRRAS spectra. Before correlation, these spectra were normalized for changes in surface density as previously described [19,28] and were baseline-corrected using the GRAMS/AI spectral software package (Galactic, Nashua, NH). Special considerations were made for baseline correction in the amide I spectral region between 1600 and 1700 cm^{-1}. Details of the procedures used in this region are presented in the Appendix A. The 2D plots presented in this article were calculated using two-dimensional *kv* correlation analysis algorithms written in our laboratory for the MATLAB programming environment (Version 6, The MathWorks, Natick, MA).

3. Results and discussion

3.1. Pure mSP-$B_{1–25}$ peptide monolayers

We have used polarization modulation infrared reflectance spectroscopy (PM-IRRAS) to study the structure and orientation of the mSP-$B_{1–25}$ peptide as an individual monolayer film at the A/W interface as well as when inserted in 4:1 DPPC-d_{62}:DOPG monolayers at different concentrations (10, 5 and 1 wt.%). PM-IRRAS has several advantages over conventional polarized IR reflectance spectroscopy for the study of monolayer films at the A/W interface, specifically the ability to discriminate against isotropic water and water vapor absorptions and the ability to analyze the resulting spectra directly for the orientation and conformation of the interfacial monolayer [29].

Fig. 1 shows the amide I region in the PM-IRRAS spectrum of a monomolecular film containing only mSP-$B_{1–25}$ on a 120 mM NaCl subphase. The spectra were collected at increasing surface pressures between 1 and 25 mN/m. The predominant intensity of the broad amide band is seen at 1658 cm^{-1}, corresponding to an α-helical component of peptide structure. The surface selection rules of the PM-IRRAS experiment at the air–water interface specify that strong positive absorption bands in the spectrum indicate IR transition dipole moments that are aligned parallel to the interface [18]. If it is assumed that the amide I dipole moment of the peptide is oriented in the plane of the surface, this implies that the mSP-$B_{1–25}$ peptide is oriented approximately 29°–38° from the interface (depending on the choice of the angle between the amide I transition moment and the long axis of the α-helix). An orientation angle of 29°–38° from the horizontal is consistent with the tilt angle for SP-$B_{1–25}$ (56° from the normal to the interface)

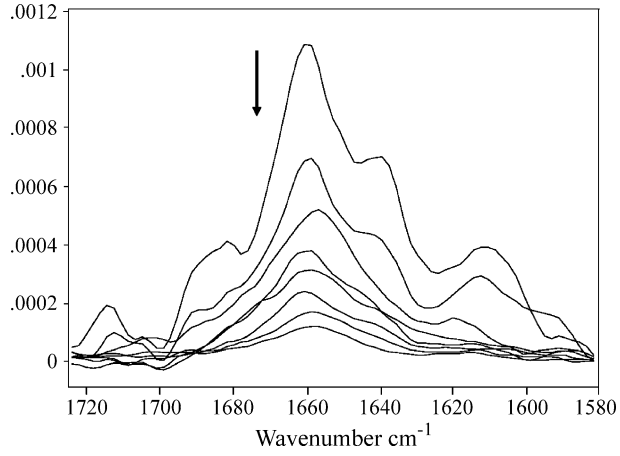

Fig. 1. PM-IRRAS spectra of a monomolecular film of mSP-$B_{1–25}$ at the A/W interface. Spectra were collected at surface pressures ranging between 1 and 25 mN/m as the monolayer was compressed. The spectral region between 1730 and 1580 cm^{-1} showing the peptide amide I band is displayed. The direction of the arrow indicates a decrease of spectral intensity in the amide I band upon monolayer compression. Monolayers were studied at 22±0.3 °C at the A/W interface on a subphase containing 120 mM NaCl.

calculated from X-ray scattering [13]. The intensity of the amide I band in the IRRAS spectra for the mSP-$B_{1–25}$ peptide monolayer in Fig. 1 decreases with increasing surface pressure, indicating that the orientation of the dipole moment changes from being parallel to perpendicular with respect to the interface.

An earlier IRRAS study of a shorter SP-$B_{1–20}$ monolayer on a D_2O subphase has reported an amide I band frequency at 1642 cm^{-1} indicative of a solvent-exposed α-helical or random coil structure [30]. Based on the broadness of the amide I band, the authors also suggested a small degree of β-sheet structure or surface aggregation in the peptide monolayer. A reversible surface pressure-induced β-sheet structure has also been reported for a SP-$B_{9–36}$ peptide [10,30]. In order to address the secondary structure of mSP-$B_{1–25}$ at the A/W interface more quantitatively, we applied *kv* correlation analysis to the measured PM-IRRAS spectra. (Note: A detailed description of the data analysis methods we used to process the PM-IRRAS spectra, including an explanation of the *kv* correlation analysis technique, is provided in Appendix A.)

Fig. 2 shows the *kv* correlation plot calculated from PM-IRRAS spectra for an mSP-$B_{1–25}$ monolayer as a function of surface pressure. The peaks in the upper panel reflect correlations having a positive intensity, and those in the lower panel correspond to negative correlation intensity. The peaks in the *kv* correlation plot in Fig. 2 confirm that mSP-$B_{1–25}$ has heterogeneous structural regions during compression. Specific band assignments and calculated k_{eff} values from the spectra in Fig. 2 are given in Table 1. Positive correlation peaks are observed at 1688.7 (β-sheet), 1660.2 (α-helix), 1637.6 (β-turn) and 1608 cm^{-1} (side chain). Negative correlation peaks are observed at 1688.7

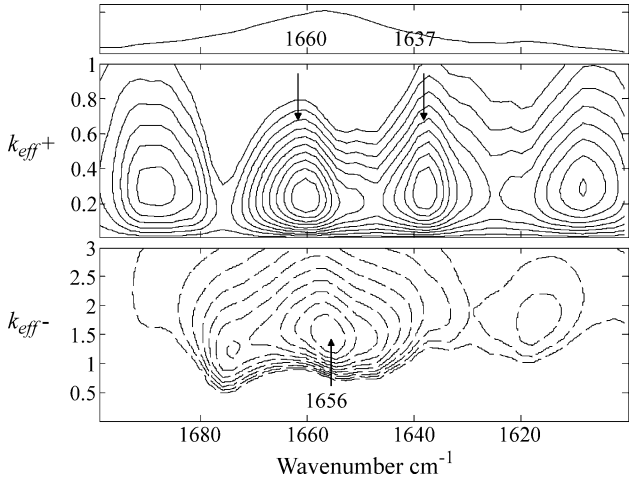

Fig. 2. *kv* correlation plots calculated from the PM-IRRAS spectra of a monolayer of mSP-$B_{1–25}$ displayed in Fig. 1. Solid lines indicate regions of positive correlation intensity; dashed lines indicate regions of negative correlation intensity. The one-dimensional spectrum shown on the top is a representative spectrum taken from the data set used in the *kv* analysis. Upper panel represents positive exponential correlation values (k_{eff}^{+}) while the lower panel indicates negative exponential correlation values (k_{eff}^{-}).

Table 1
Band assignments and values of effective rate constants (k_{eff}) for monolayers of pure mSP-$B_{1–25}$ at the A/W interface

Wavenumber, cm^{-1}	Assignment	k_{eff}+	k_{eff}−
1688.7	β-sheet	0.28	2.23
1674.2	β-turn	–	1.22
1660.2	α-helix	0.23	–
1656.0	α-helix	–	1.49
1637.6	β-turn	0.28	–
1617.1	β-sheet	–	1.78
1608.0	Side Chain	0.30	–

Tabulated values of k_{eff} were calculated from the *kv* correlation plot in Fig. 2 in conjunction with PM-IRRAS spectra for pure mSP-$B_{1–25}$ monolayers at the A/W interface.

(β-sheet), 1674.2 (β-turn), 1656 (α-helix) and 1617 cm^{-1} (β-sheet). The positive peak at 1660 cm^{-1} is assumed to reflect α-helical structure, but shifted somewhat in frequency due to changes in peptide orientation during monolayer compression. Based on the above, the secondary structure of pure mSP-$B_{1–25}$ at the A/W interface contains a substantial component of α-helix together with regions of β-sheet.

In addition to identifying specific structural components in the amide band contour, *kv* correlation analysis also assesses the rate at which these components change relative to one another as surface pressure increases during compression [24]. For the mSP-$B_{1–25}$ peptide at the A/W interface, the values of k_{eff} in Table 1 show that vibrations attributed to regions of β structure have larger k_{eff} values and hence reorient earlier during compression than the α-helical portion of the peptide.

3.2. Monolayers containing DPPC-d_{62}:DOPG+10 wt.% mSP-$B_{1–25}$

PM-IRRAS spectra for monolayers containing 4:1 DPPC-d_{62}:DOPG plus 10 wt.% mSP-$B_{1–25}$ are shown in Fig. 3. The spectra were collected at increasing surface pressures between 1 and 50 mN/m during monolayer compression. The bands that are most prominent in the spectrum in Fig. 3A are at 1737 cm^{-1} (C=O stretching vibration of the DPPC-d_{62} and DOPG carbonyl bands), 1658 cm^{-1} (amide I band of the mSP-$B_{1–25}$ peptide), 1265 cm^{-1} (asymmetric PO_4^{2-} stretching vibration of the phospholipids), 1220 cm^{-1} (asymmetric PO_4^{2-} stretching vibration of the phospholipids), 1085 cm^{-1} (combination of the symmetric PO_4^{2-} stretching vibration of phospholipids and the CD_2 scissoring mode of DPPC-d_{62}) and 1053 cm^{-1} (asymmetric carbonyl ester stretch due to the phospholipids). Fig. 3B shows only those vibrations due to the carbonyl group of the phospholipids and the amide I band of the peptide in the 1820–1550 cm^{-1} spectral region. The positive PM-IRRAS absorption bands of the amide I and carbonyl bands indicate that their transition dipole moments are aligned parallel to the interface [18]. The intensity of the amide I band is also seen to decrease with increasing surface

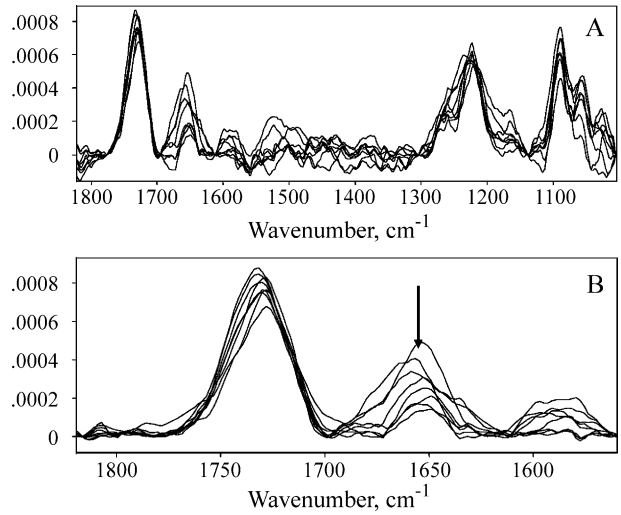

Fig. 3. PM-IRRAS spectra of a monolayer of 4:1 DPPC-d_{62}:DOPG containing 10% mSP-$B_{1–25}$ at the A/W interface. Spectra were collected at surface pressures ranging between 1 and 50 mN/m as the monolayer was compressed at 22±0.3 °C at the A/W interface on a subphase of 120 mM NaCl. (A) Spectral region between 1800 and 1000 cm^{-1}; (B) Spectral region between 1820 and 1550 cm^{-1} that incorporates the lipid carbonyl C=O stretching band (~1740 cm^{-1}) and the peptide amide I band (~1650 cm^{-1}). The direction of the arrow indicates a decrease in the spectral intensity of the amide I band upon monolayer compression.

pressure, indicating that the orientation of the dipole moment changes from parallel to perpendicular to the interface during compression.

Fig. 4 shows the *kv* correlation plot of the PM-IRRAS spectra for the 10 wt.% mSP-$B_{1–25}$ mixture, while Table 2 gives band assignments and k_{eff} values for the correlation peaks. Intense negative correlation peaks were observed at 1665.1 (β-turn) and 1635.8 cm^{-1} (β-turn) and positive

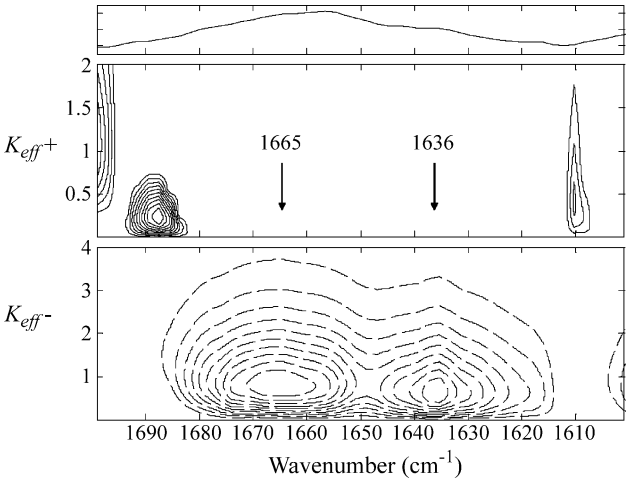

Fig. 4. *kv* correlation plots calculated from the PM-IRRAS spectra of a monolayer of 10 wt.% mSP-$B_{1–25}$ displayed in Fig. 3. Solid lines indicate regions of positive correlation intensity; dashed lines indicate regions of negative correlation intensity. The one-dimensional spectrum shown on the top is a representative spectrum taken from the data set used in the *kv* analysis. Upper panel represents positive exponential correlation values (k_{eff}^{+}) while the lower panel indicates negative exponential correlation values (k_{eff}^{-}).

Table 2
Band assignments and values of effective rate constants (k_{eff}) for monolayers of 4:1 DPPC-d_{62}:DOPG containing 10 wt.% mSP-$B_{1–25}$ at the A/W interface

Wavenumber, cm^{-1}	Assignment	k_{eff}+	k_{eff}−
1687.6	β-sheet	0.24	–
1665.1	β-turn	–	0.78
1635.8	β-turn	–	0.62
1610.1	Side chain	0.41	–

Tabulated values of k_{eff} were calculated from the *kv* correlation plot in Fig. 4 in conjunction with PM-IRRAS spectra for monolayers of 4:1 DPPC-d_{62}:DOPG plus 10 wt.% mSP-$B_{1–25}$ at the A/W interface.

correlation peaks are observed at 1687.6 (β-sheet) and 1610.1 cm^{-1} (side chain). The most striking difference between the *kv* correlation plots of mSP-$B_{1–25}$ alone (Fig. 2) and in the presence of 4:1 DPPC:DOPG (Fig. 4) is the lack of any significant correlation peak around 1655–60 cm^{-1}, wavenumbers corresponding to an α-helix. Combining 10 wt.% mSP-$B_{1–25}$ in a film with 4:1 DPPC:DOPG thus appears to induce an α-helix→β-sheet conformational change in the peptide at the A/W interface. Upon increasing surface pressure, all the secondary structural components reorient away from the interface in a coherent manner during compression.

3.3. Monolayers containing DPPC-d_{62}:DOPG+5 wt.% mSP-$B_{1–25}$

The PM-IRRAS spectra of mixed monolayers of 4:1 DPPC-d_{62}:DOPG+5 wt.% mSP-$B_{1–25}$ are presented in Fig. 5. The spectral region consisting of the amide I band (~1655 cm^{-1}) and the carbonyl band (1737 cm^{-1}) due to the

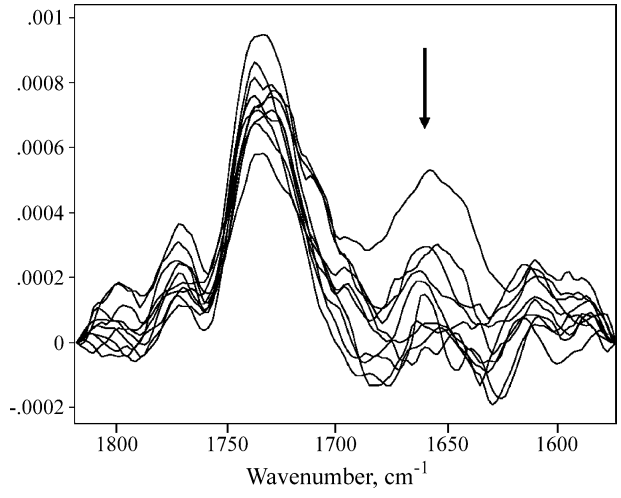

Fig. 5. PM-IRRAS spectra of a monolayer of 4:1 DPPC-d_{62}:DOPG containing 5 wt.% mSP-$B_{1–25}$ at the A/W interface. Spectra were collected at surface pressures ranging between 1 and 50 mN/m as the monolayer was compressed at 22±0.3 °C at the A/W interface on a subphase of 120 mM NaCl. Spectral region between 1820 and 1550 cm^{-1} includes the lipid carbonyl C=O stretching band (~1740 cm^{-1}) and the peptide amide I band (~1650 cm^{-1}). The direction of the arrow indicates decreased spectral intensity in the amide I band upon monolayer compression.

phospholipids are the main bands shown. The amide I band decreased in intensity as surface pressure increased, indicating a reorientation of the dipole moment of the peptide away from the interface and towards the surface normal. The *kv* correlation plot calculated from the PM-IRRAS spectra for the DPPC-d_{62}:DOPG/5 wt.% mSP-$B_{1–25}$ monolayer is shown in Fig. 6, with band assignments and corresponding k_{eff} values in Table 3. Positive correlation peaks were observed at 1641.3 (β-turn), 1618.5 (β-sheet) and 1609.4 cm^{-1} (side chain), while negative correlation peaks were observed at 1680.3 (β-sheet), 1666.3 (β-turn), 1657.0 (α-helix) and 1633.3 cm^{-1} (β-sheet). Unlike the 10 wt.% mSP-$B_{1–25}$ mixture above, a correlation cross peak at 1657 cm^{-1} was found to be present (Fig. 6), indicating that a significant segment of the peptide was in an α-helical conformation.

Calculated k_{eff} values for DPPC-d_{62}:DOPG/5 wt.% mSP-$B_{1–25}$ monolayers indicated that both the β-sheet and α-helix components have very similar rate constants (k_{eff}~0.60–0.65; Table 3). This implies little or no preferential reorientation of mSP-$B_{1–25}$ structural components during compression, with the peptide as a whole reorienting toward the surface normal as surface pressure increases. This behavior is different from that found in 10 wt.% peptide films, and reinforces the understanding that the molecular structure of SP-B can vary depending on the lipid environment, the lipid/protein ratio, the extent of film compression and other factors [19,31–33].

3.4. Monolayers containing DPPC-d_{62}:DOPG+1 wt.% mSP-$B_{1–25}$

Fig. 7A shows PM-IRRAS spectra for monolayers containing 4:1 DPPC-d_{62}:DOPG+1 wt.% mSP-$B_{1–25}$ on a

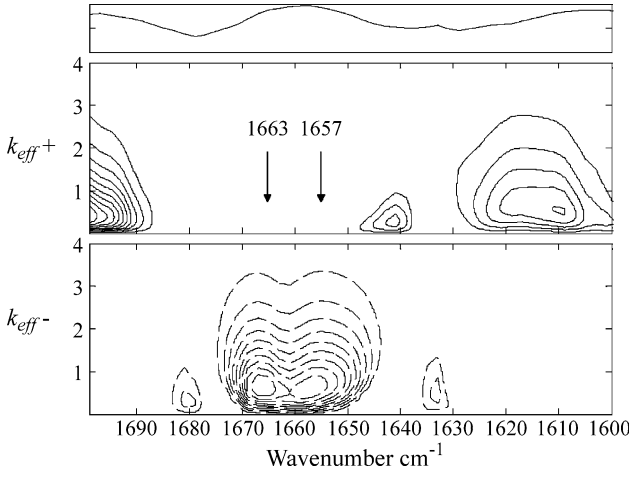

Fig. 6. *kv* correlation plots calculated from the PM-IRRAS spectra of a monolayer of 5 wt.% mSP-$B_{1–25}$ displayed in Fig. 5. Solid lines indicate regions of positive correlation intensity; dashed lines indicate regions of negative correlation intensity. The one-dimensional spectrum shown on the top is a representative spectrum taken from the data set used in the *kv* analysis. Upper panel represents positive exponential correlation values (k_{eff}^{+}) while the lower panel indicates negative exponential correlation values (k_{eff}^{-}).

Table 3
Band assignments and values of effective rate constants (k_{eff}) for monolayers of 4:1 DPPC-d_{62}:DOPG containing 5 wt.% mSP-$B_{1–25}$ at the A/W interface

Wavenumber, cm^{-1}	Assignment	k_{eff}+	k_{eff}−
1680.3	β-sheet	–	0.31
1666.3	β-turn	–	0.65
1657.0	α-helix	–	0.60
1641.3	β-turn	0.28	–
1633.3	β-sheet	–	0.52
1618.5	β-sheet	0.65	–
1609.4	Side chain	0.55	–

Tabulated values of k_{eff} were calculated from the *kv* correlation plot in Fig. 6 in conjunction with PM-IRRAS spectra for monolayers of 4:1 DPPC-d_{62}:DOPG plus 5 wt.% mSP-$B_{1–25}$ at the A/W interface.

subphase of 120 mM NaCl. As in the more concentrated peptide films above, the intensity of the amide band decreased with increasing surface pressure, indicating an overall reorientation of the dipole moment of the peptide towards the surface normal. Fig. 8 shows the *kv* correlation plot calculated from the PM-IRRAS spectra for the 4:1 DPPC-d_{62}:DOPG/1 wt.% mSP-$B_{1–25}$ monolayer, and Table 4 shows the band assignments and corresponding k_{eff} values. Positive correlation peaks were found at 1686.9 (β-sheet), 1678.2 (β-turn) and 1652.6 cm^{-1} (α-helix), while negative correlation peaks were present at 1696.8 (side chain), 1686.9 (β-sheet), 1668.5 (β-turn), 1637.4 (β-turn), 1630.5 (β-sheet), 1621.3 (β-sheet) and 1602.4 cm^{-1} (side

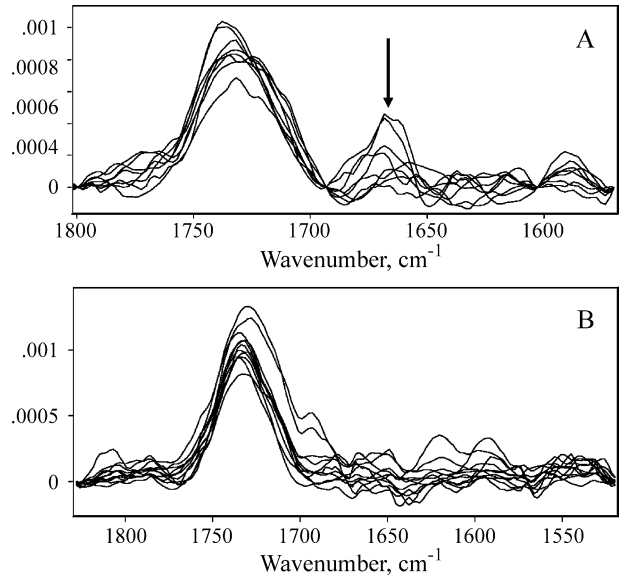

Fig. 7. PM-IRRAS spectra of a monolayer of 4:1 DPPC-d_{62}:DOPG containing 1% mSP-$B_{1–25}$ at the A/W interface. Spectra were collected at surface pressures ranging between 1 and 50 mN/m as the monolayer was compressed at 22±0.3 °C. The spectral region between 1820 and 1550 cm^{-1} shows the lipid carbonyl C=O stretching band (~1740 cm^{-1}) and the peptide amide I band (~1650 cm^{-1}). (A) Monolayer on a subphase containing 120 mM NaCl; (B) Monolayer on a subphase containing 120 mM NaCl plus 2 mM $CaCl_2$. Direction of the arrow in panel (A) indicates a decrease of spectral intensity for the amide I band upon monolayer compression.

chain). The most notable aspect of the correlation analysis in Fig. 8 is the intense correlation peak at 1652.6 cm^{-1} with k_{eff}=+0.31, indicating a strong positive correlation for an α-helical peptide conformation in the 1 wt.% mSP-$B_{1–25}$ monolayer. The 2D IR correlation analyses in Figs. 4, 6 and 8) unambiguously show that the conformation of mSP-$B_{1–25}$ in monolayers with 4:1 DPPC-d_{62}:DOPG is concentration-dependent. At higher peptide levels (10 wt.%), the predominant secondary structural peptide conformation is β-sheet. As the concentration of the peptide decreases towards physiological values of 1 wt.%, the mSP-$B_{1–25}$ peptide adopts a much more markedly α-helical conformation within the surface film.

The calculated k_{eff} values for DPPC-d_{62}:DOPG/1 wt.% mSP-$B_{1–25}$ monolayers also show that the different secondary structural components of the peptide have divergent rate constants as a function of surface pressure (Table 4). This behavior differs from the data for monolayers containing 5 wt.% mSP-$B_{1–25}$ (Table 3), and indicates that the α and β peptide structural components in 1 wt.% monolayers reorient independently during compression. The β structural components have consistently larger k_{eff} values (0.95–0.17) than the α-helical structures (k_{eff}~0.31), indicating an initial reorientation of β secondary structure with increasing surface pressure, followed by a slower reorientation of α-helix.

A recent fluorescence quenching study on the topographical organization of the mSP-$B_{1–25}$ peptide incorporated in DPPC liposomes has proposed that the α-helical peptide regions are aligned parallel to the water–lipid interface [34], although earlier physical [15,22] and computational studies [14] have postulated a tilted peptide model. The data presented here indicate that for all

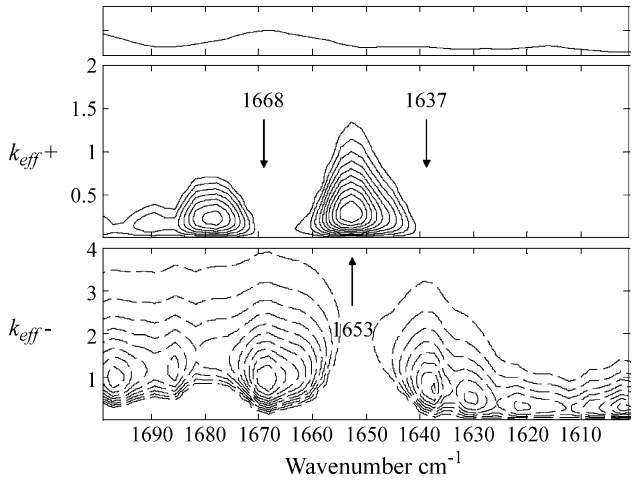

Fig. 8. *kv* correlation plots calculated from the PM-IRRAS spectra of a monolayer of 1 wt.% mSP-$B_{1–s25}$ displayed in Fig. 7 (A). The solid lines indicate regions of positive correlation intensity; and the dashed lines indicate regions of negative correlation intensity. The one-dimensional spectrum shown at the top is representative of the data used in *kv* analysis. The upper panel represents positive exponential correlation values (k_{eff}^{+}) while the lower panel indicates negative exponential correlation values (k_{eff}^{-}).

Table 4
Band assignments and values of effective rate constants (k_{eff}) for monolayers of 4:1 DPPC-d_{62}:DOPG containing 1 wt.% mSP-$B_{1–25}$ at the A/W interface

Wavenumber, cm^{-1}	Assignment	k_{eff}+	k_{eff}−
1696.8	Side chain		1.03
1686.9	β-sheet	0.18	1.17
1678.2	β-sheet	0.23	–
1668.5	β-turn	–	0.95
1652.6	α-helix	0.31	–
1637.4	β-turn	–	0.76
1630.5	β-sheet	–	0.50
1621.3	β-sheet	–	0.31
1602.4	Side chain	–	0.31

Tabulated values of k_{eff} were calculated from the *kv* correlation plot in Fig. 8 in conjunction with PM-IRRAS spectra for monolayers of 4:1 DPPC-d_{62}:DOPG plus 1 wt.% mSP-$B_{1–25}$ at the A/W interface.

concentrations tested, the mSP-$B_{1–25}$ peptide is oriented in the plane of the interface only at low surface pressures, and becomes increasingly upright and oriented away from the interface with increasing surface pressure.

3.5. Monolayers containing DPPC$_{d62}$:DOPG+1 wt.% mSP-B$_{1–25}$ on 2 mM CaCl$_2$

The presence of 2 mM Ca^{2+} was found to have little or no effect on the PM-IRRAS spectra or *kv* correlation plots of pure films of mSP-$B_{1–25}$ or films containing 4:1 DPPC-d_{62}:DOPG plus 10 or 5 wt.% peptide. However, this was not true for monolayers of 4:1 DPPC-d_{62}:DOPG plus 1 wt.% mSP-$B_{1–25}$ (Fig. 7B). For this mixture, the only major band observed in the PM-IRRAS spectrum in the presence of Ca^{2+} is the C=O stretching vibration at 1737 cm^{-1} due to the phospholipids (Fig. 7B). The prominent amide I band in Fig. 7A on a subphase containing only 120 mM NaCl is notably absent in Fig. 7B. The absence of the amide signal in the Ca^{2+}-containing system is consistent with either an isotropic monomolecular film or a preferred peptide orientation in which the transition dipole moment has coexisting positive and negative signal contributions that cancel each other [29]. Moreover, the DPPC-d_{62}:DOPG/1 wt.% mSP-$B_{1–25}$ film in Fig. 7B exhibits no discernable change in amide I band intensity as surface pressure increases, indicating that Ca^{2+} has locked the peptide α-helix into an immobile conformation that resists reorientation. The calcium-dependent IR behavior of 4:1 DPPC:DOPG monolayers containing 1 wt.% mSP-$B_{1–25}$ is consistent with the finding that these monolayers display differing fluorescence images when studied on subphases with and without 2 mM Ca^{2+} [17].

4. Conclusions

Research over the past several decades has examined and established the functional importance of lung surfactant

proteins in vivo and in clinical exogenous surfactants. Only a portion of the molecular structure of full length SP-B is reflected in the mSP-$B_{1–25}$ peptide studied here. Each monomer of the complete native SP-B protein contains three intramolecular disulfide bridges that impart considerable structural rigidity. An intermolecular disulfide-linked dimer form is also prevalent in humans and other animal species, and higher oligomers also exist including trimers and possibly even salt bridge-linked quaternary forms. However, despite containing only a portion of the structure of the native protein, monomer and dimer peptides incorporating the 25 N-terminal residues of human SP-B mimic many of its surface active and biophysical behaviors [35–43]. The results of the present study are consistent with and extend this prior work, demonstrating extensive structurally-relevant molecular interactions of mSP-$B_{1–25}$ in mixed films with 4:1 DPPC:DOPG at the A/W interface.

To date, there have been relatively few spectroscopic studies that have directly addressed the conformation and configuration of SP-B in monolayers. One such study used grazing angle X-ray diffraction to examine mSP-$B_{1–25}$ in fatty acid monolayers [13], and reported that the peptide was oriented at an angle of ~56° relative to the surface normal. However, the grazing angle X-ray approach only indirectly addresses protein conformation, as it monitors the ordered phase of the monolayer and implicitly describes peptide configuration based on the changes in order. IR spectroscopic methods can address the conformation of proteins in monomolecular films with more direct specificity. External reflectance IR spectroscopy was initially used to study molecular structure in films at the A/W interface in the mid-1980s, and progress in this field has recently been reviewed [44,45]. The technique can also be extended by the use of polarization–source modulation using a photoelastic modulator [18]. IRRAS methodology has previously been applied to study surfactant films at the A/W interface, including studies on extracted lung surfactant [46]. More recently, IRRAS has been used to investigate the functional roles of the hydrophobic surfactant proteins SP-B and pulmonary surfactant protein C (SP-C) [20,47–49]. PM-IRRAS and 2D IR correlation methods have recently been used to examine the molecular behavior of native SP-B and SP-C in monolayers, demonstrating that these proteins adopt a variety of conformations and orientations during compression [19]. However, the present studies are the first to address specific conformations and orientations of the N-terminal region of human SP-B directly in compressed films with phospholipids at the A/W interface.

Several prior IR studies have investigated the secondary structure of N-terminal SP-B peptides. A bulk phase IR study of ^{13}C-labelled mSP-$B_{1–25}$ indicated a predominately α−helical peptide structure in solution and in liposomes [11]. An earlier IRRAS study of an SP-B peptide fragment (SP-$B_{1–20}$) on a D_2O subphase observed the amide I band frequency at 1642 cm^{-1} indicative of a solvent-exposed α-helical or random coil structure [29]. Based on the broadness of the amide I band, the authors also suggested that a small degree of β-sheet structure or surface aggregation should also be present in the SP-$B_{1–20}$ monolayer. In addition, they also examined an SP-$B_{9–36}$ peptide and showed that it could undergo a reversible surface-pressure induced formation of β-sheet structure in the peptide monolayer. The reversible formation of β-sheet structure in an SP-$B_{9–36}$ peptide has recently been confirmed using ^{13}C-labelling [10].

The current study has examined the conformation and orientation of mSP-$B_{1–25}$ in monolayers at the A/W interface, both as a pure substance and in mixtures with 4:1 DPPC-d_{62}:DOPG containing peptide contents of 1–10 wt.%. The lower 1 wt.% concentration level closely mimics the physiological content of hydrophobic proteins in endogenous lung surfactant. The results here are the first to directly examine the conformation of mSP-$B_{1–25}$ peptide in a DPPC:DOPG matrix at the A/W interface. A model-dependent 2D IR correlation analysis method (*kv* correlation analysis) recently developed in our laboratory [24] was used to reveal rate relationships involving the molecular conformation and reorientation of mSP-$B_{1–25}$ in compressed interfacial films. A different 2D IR correlation analysis method was previously been applied to the IRRAS spectra of full-length SP-B and SP-C [19]. In the present study, a combination of PM-IRRAS and *kv* correlation analysis showed that in monolayers at the A/W interface, pure mSP-$B_{1–25}$ had a heterogeneous secondary structure dominated by α-helix but also containing β-sheet structure (Figs. 1 and 2). Calculated values of k_{eff} for β-sheet structural regions in pure mSP-$B_{1–25}$ monolayers were larger than those of α-helical structural regions, indicating an earlier reorientation of the β structures with increasing surface pressure during compression.

Our results also show that the conformation and reorientation of mSP-$B_{1–25}$ was strongly affected by incorporation in a phospholipid matrix at the A/W interface. A comparison of *kv* correlation analyses from Figs. 4, 6 and 8) shows unambiguously that the conformation of the mSP-$B_{1–25}$ peptide in 4:1 DPPC-d_{62}:DOPG monolayers was concentration-dependent. In films of 4:1 DPPC:DOPG plus 10 wt.% mSP-$B_{1–25}$, there was a lack of any significant correlation peak around 1655–60 cm^{-1} corresponding to an α-helix (compare Figs. 2 and 4). During compression, all of the peptide secondary structural components in films containing 10 wt.% mSP-$B_{1–25}$ became reoriented away from the interface in a coherent manner as surface pressure increased. The extent of peptide α-helical structures in surface films with 4:1 DPPC:DOPG became more substantial as mSP-$B_{1–25}$ content was reduced to physiological levels. At mSP-$B_{1–25}$ contents of 5 wt.%, a correlation cross peak at 1657 cm^{-1} appeared in the *kv* correlation analysis plot (Fig. 6), indicating a substantial segment of the peptide in an α-helical conformation. However, k_{eff} rate constants for this film implied no preferential reorientation of secondary structure components as the peptide as a whole

reoriented toward the surface normal with increasing surface pressure (Table 3). In phospholipid monolayers containing 1 wt.% mSP-B_{1-25}, an intense correlation peak at 1652.6 cm^{-1} with k_{eff}=+0.31 indicated a very strong positive correlation for an α-helical conformation (Fig. 8). Moreover, in the 1 wt.% film, divergent k_{eff} values indicated that the structural components of the peptide reoriented independent of one another as surface pressure increased during compression (Table 4). Calculated k_{eff} values for 1 wt.% peptide films were consistent with an initial reorientation of β-structure secondary structure with increasing surface pressure, followed by a slower reorientation of α-helical regions of peptide structure.

Acknowledgements

The financial support of the U.S. Public Health Service through National Institutes of Health (NIH) grants EB001956 (R.A.D.), HL56176 (R.H.N.) and HL55534 (F.J.W. and A.J.W.) is gratefully acknowledged.

Appendix A. 2D IR correlation analysis of PM-IRRAS spectra of peptides - data analysis methods

The analysis of PM-IRRAS spectra of peptides at the A/W interface requires careful spectral data processing. PM-IRRAS spectra possess a strong downward sloping baseline between 1700 and 1650 cm^{-1} due to the anomalous dispersion of the real part of the refractive index of water in this region, arising from the δ(H-O-H) deformation vibration of liquid water [29]. The intensity of this deformation vibration increases as the monolayer is compressed to higher surface pressures due to a change in the structure of the water molecules at the interface. In 2D IR correlation analysis, one of the requisite data pretreatment methods is to ensure a uniform baseline for all the spectra. Therefore, baseline correction of monolayer PM-IRRAS spectra, especially in the amide I region, is needed. We accomplished baseline correction for the amide I bands by fitting a Lorentzian curve to the δ(H–O–H) deformation band and subtracting this band from each of the experimentally acquired PM-IRRAS spectra. The full-width at half maximum of the Lorentzian band was varied depending on the surface tension and the resulting shape of the δ(H–O–H) spectral feature. The baseline-corrected PM-IRRAS spectra were then normalized for changes in surface density. These baseline-corrected and normalized spectra were used in the 2D IR correlation analyses described in this article to determine the structure and orientation of mSP-B_{1-25} in a pure component film at the A/W interface as well as when inserted in 4:1 DPPC-d_{62}:DOPG monolayers at different concentrations (10, 5 and 1 wt.%).

Two-dimensional infrared correlation spectroscopy (2D IR) has been shown to be a very effective technique in elucidating secondary structural information from infrared absorption spectra of proteins undergoing a dynamic perturbation [50–52]. This dynamic environmental perturbation could be the concentration of the protein, temperature, pH of the solvent or, as in the current case, surface pressure. In a previous publication, we successfully applied both conventional and modified 2D IR to IRRAS spectra of surfactant protein (SP-C) monolayers. These methods allowed us to identify protein secondary structural components and assign relative rates of orientation as a function of monolayer compression for those components [19].

In the current analysis of the PM-IRRAS spectra of mSP-B_{1-25} at the A/W interface, we have used a method known as *kν* correlation analysis to evaluate the spectra. A *kν* correlation analysis is a mathematical asynchronous cross-correlation performed between a set of *N* spectra undergoing some dynamic intensity variation against a set of exponential functions with a user-defined range of rate constants. Details of the *kν* correlation analysis method are presented elsewhere [24]. The *kν* correlation analysis method is a model-dependent 2D IR correlation method analogous to the β*ν* method we previously used to analyze monolayer IR spectra of the native SP-B and SP-C proteins [19]. In *kν* correlation analysis, the observed correlation intensities are a function of the rate constant of the exponential function and the spectral frequency. The 2D correlation plots reveal rate relationships between different molecular events in terms of a quantitative and tangible parameter, *k*, which is the rate constant of the exponential function used in the correlation. A new parameter, the effective rate constant, k_{eff}, is defined as the point of maximum correlation intensity at particular frequencies in the plot of *k* vs. í. The calculated values of k_{eff} represent the rates at which the intensities of the spectral bands change during the course of the dynamic experiment. As a result, these k_{eff} values are comparable and can be used to assign quantitative rate relationships. Events at frequencies with a larger k_{eff} value occur earlier than events at frequencies with smaller k_{eff} values. Positive and negative k_{eff} values are comparable and hence no manipulation of the spectra or the correlation plots is required to compare bands with increasing and decreasing intensities.

We have shown that *kν* correlation methods are sensitive to the relative change in the rates of the band intensities through a dynamic data set [24]. The k_{eff} values are not the actual kinetic rate constants per se, instead the k_{eff} parameter is sensitive to the relative order in which the intensity change occurs, while the size of the correlation peaks gives an indication of the magnitude of the intensity change. Spectral bands whose rate of intensity change varies through a dynamic data set are distinguished by the presence of both positive and negative peaks in the *kν* correlation plots.

The presence of both a positive and negative correlation peak at a particular frequency can be understood as a modulation in the rate of intensity change at that frequency. The decrease in intensity of the amide I band upon increasing surface pressure in the PM-IRRAS spectra of

mSP-B_{1-25} (Fig. 7) suggest that the positive peaks in the correlation plot are due to a decreased rate of change in these bands with increasing surface pressure. Because the PM-IRRAS spectra used in the $k\nu$ correlation analysis have already been normalized for changes in surface density, the correlation peak intensity can be taken as an indicator of the change in intensity as a result of change in orientation of the amide I band.

References

[1] Y. Tanaka, T. Takei, T. Aiba, K. Masuda, A. Kiuchi, T. Fujiwara, Development of synthetic lung surfactants, J. Lipid Res. 27 (1986) 475–485.

[2] F.R. Poulain, J.A. Clements, Pulmonary surfactant therapy, West. J. Med. 162 (1995) 43–50.

[3] S. Hawgood, M. Derrick, P. Poulain, Structure and properties of surfactant protein B, Biochim. Biophys. Acta 1408 (1998) 150–160.

[4] R. Veldhuizen, K. Nag, S. Orgeig, F. Possmayer, The role of lipids in pulmonary surfactant, Biochim. Biophys. Acta 1408 (1998) 90–108.

[5] R.H. Notter, Lung Surfactants: Basic Science and Clinical Applications, Marcel Dekker, New York, 2000.

[6] P. Chess, J.N. Finkelstein, B.A. Holm, R.H. Notter, Surfactant replacement therapy in lung injury, in: R.H. Notter, J.N. Finkelstein, B.A. Holm (Eds.), Lung Injury: Mechanisms, Pathophysiology and Therapy, Marcel Dekker, New York, 2005, in press.

[7] A.J. Waring, K.F. Faull, C. Leung, A. Chang-Chien, P. Mercado, H.W. Taeusch, L.M. Gordon, Synthesis, secondary structure and folding of the bend region of lung surfactant protein B, Pept. Res. 9 (1996) 28–39.

[8] E. Liepinsh, M. Andersson, J.-M. Ruysschaert, G. Otting, Saposin fold revealed by the NMR structure of NK-lysin, Nat. Struct. Biol. 4 (1997) 793–795.

[9] S. Zaltash, M. Palmblad, T. Curstedt, J. Johansson, B. Persson, Pulmonary surfactant protein B: a structural model and a functional analogue, Biochim. Biophys. Acta 1466 (2000) 179–186.

[10] C.R. Flach, P. Cai, D. Dieudonne, J.W. Brauner, K.M.W. Keough, J. Stewart, R. Mendelsohn, Location of structural transitions in an isotopically labeled lung surfactant SP-B peptide by IRRAS, Biophys. J. 85 (2003) 340–349.

[11] L.M. Gordon, K.Y.C. Lee, M.M. Lipp, J.A.N. Zasadzinski, F.J. Walther, M.A. Sherman, A.J. Waring, Conformational mapping of the N-terminal segment of surfactant protein B in lipid using ^{13}C-enhanced Fourier transform infrared spectroscopy, J. Pept. Res. 55 (2000) 330–347.

[12] B.N. Flanders, S.A. Vickery, R.C. Dunn, Imaging of monolayers composed of palmitic acid and lung surfactant protein B, J. Microsc. 202 (2001) 379–385.

[13] K.Y. Lee, J. Majewski, T.L. Kuhl, P.B. Howes, K. Kjaer, M.M. Lipp, A.J. Waring, J.A.N. Zasadzinski, G.S. Smith, Synchrotron X-ray study of lung surfactant-specific protein SP-B in lipid monolayers, Biophys. J. 81 (2001) 572–585.

[14] Y.N. Kaznessis, S. Kim, R.G. Larson, Specific mode of interaction between components of model pulmonary surfactants using computer simulations, J. Mol. Biol. 322 (2002) 569–582.

[15] J.W. Kurutz, K.Y.C. Lee, NMR structure of lung surfactant peptide SP-B_{11-25}, Biochemistry 41 (2002) 9627–9636.

[16] J.A. Freites, Y. Choi, D.J. Tobias, Molecular dynamics simulations of a pulmonary surfactant protein B peptide in a lipid monolayer, Biophys. J. 84 (2003) 2169–2180.

[17] N. Biswas, S. Shanmukh, A. Waring, F.J. Walther, Z. Wang, Y. Chang, R.H. Notter, R.A. Dluhy, Structure and properties of phospholipid–peptide monolayers containing monomeric SP-B_{1-25} I. Phases and morphology by epi-fluorescence microscopy, Biophys. Chem. 113 (2004) 223–232, doi:10.1016/j.bpc.2004.09.008.

[18] D. Blaudez, T. Buffeteau, J.C. Cornut, B. Desbat, N. Escafre, M. Pezolet, J.M. Turlet, Polarization-modulated FT-IR spectroscopy of a spread monolayer at the air/water interface, Appl. Spectrosc. 47 (1993) 869–874.

[19] S. Shanmukh, P. Howell, J.E. Baatz, R.A. Dluhy, Effect of hydrophobic surfactant proteins SP-B and SP-C on phospholipid monolayers. Protein structure studied using 2D IR and bn correlation analysis, Biophys. J. 83 (2002) 2126–2141.

[20] J.M. Brockman, Z. Wang, R.H. Notter, R.A. Dluhy, Effect of hydrophobic surfactant proteins SP-B and SP-C on binary phospholipid monolayers: II. Infrared external reflectance-absorption spectroscopy, Biophys. J. 84 (2003) 326–340.

[21] C.G. Fields, D.H. Lloyd, R.L. Macdonald, K.M. Ottenson, R.L. Noble, HBTU activation for automated Fmoc solid-phase peptide synthesis, Pept. Res. 4 (1991) 95–101.

[22] L.M. Gordon, S. Horvath, M.L. Longo, J.A.N. Zasadzinski, H.W. Taeusch, K. Faull, C. Leung, A.J. Waring, Conformation and molecular topography of the N-terminal segment of surfactant protein-B in structure-promoting environments, Protein Sci. 5 (1996) 1662–1675.

[23] R.A. Dluhy, S. Shanmukh, J.B. Leapard, P. Krüger, J.E. Baatz, Deacylated pulmonary surfactant protein SP-C transforms from α-helical to amyloid fibril structure via a pH-dependent mechanism: an infrared structural investigation, Biophys. J. 85 (2003) 2417–2429.

[24] S. Shanmukh, R.A. Dluhy, kν correlation analysis. A quantitative two-dimensional IR correlation method for analysis of rate processes using exponential functions, J. Phys. Chem., A (2004) 5625–5634.

[25] D.L. Elmore, R.A. Dluhy, $\beta\nu$ correlation analysis: a modified two-dimensional infrared correlation method for determining relative rates of intensity change, J. Phys. Chem., B 105 (2001) 11377–11386.

[26] I. Noda, Two-dimensional infrared (2D IR) spectroscopy: theory and applications, Appl. Spectrosc. 44 (1990) 550–554.

[27] I. Noda, Determination of two-dimensional correlation spectra using the Hilbert Transform, Appl. Spectrosc. 54 (2000) 994–999.

[28] D.L. Elmore, R.A. Dluhy, Pressure-dependent changes in the infrared C–H vibrations of monolayer films at the air/water interface revealed by two-dimensional infrared correlation spectroscopy, Appl. Spectrosc. 54 (2000) 956–962.

[29] D. Blaudez, J.-M. Turlet, J. Dufourcq, D. Bard, T. Buffeteau, B. Desbat, Investigations at the air/water interface using polarization modulation IR spectroscopy, J. Chem. Soc., Faraday Trans. 92 (1996) 525–530.

[30] D. Dieudonne, R. Mendelsohn, R.S. Farid, C. Flach, Secondary structure in lung surfactant SP-B peptides: IR and CD studies of bulk and monolayer phases, Biochim. Biophys. Acta 1511 (2001) 99–112.

[31] A. Cruz, C. Casals, J. Perez-Gil, Conformational flexibility of pulmonary surfactant proteins SP-B and SP-C studied in aqueous–organic solvents, Biochim. Biophys. Acta 1255 (1995) 68–76.

[32] A. Cruz, C. Casals, K.M.W. Keough, J. Perez-Gil, Different modes of interaction of pulmonary surfactant protein SP-B in phosphatidylcholine bilayers, Biochem. J. 327 (1997) 133–138.

[33] A. Cruz, C. Casals, I. Plasencia, D. Marsh, J. Perez-Gil, Depth profiles of pulmonary surfactant protein B in phosphatidylcholine bilayers, studied by fluorescence and electron spin resonance spectroscopy, Biochemistry 37 (1998) 9488–9496.

[34] Y.D. Wang, K.M.K. Rao, E. Demchuk, Topographical organization of the N-terminal segment of lung pulmonary surfactant protein B (SP-B_{1-25}) in phospholipid bilayers, Biochemistry 42 (2003) 4015–4027.

[35] B. Fan, R. Bruni, W. Taeusch, R. Findlay, A. Waring, Antibodies against synthetic amphipathic helical sequences of surfactant protein SP-B detect a conformational change in the native protein, FEBS Lett. 282 (1991) 220–224.

[36] M.L. Longo, A.M. Bisagno, J.A. Zasadzinski, R. Bruni, A.J. Waring, A function of lung surfactant protein SP-B, Science 261 (1993) 453–456.

[37] M.L. Longo, A.M. Bisagno, J.A.N. Zasadzinski, R. Bruni, A.J. Waring, A function of lung surfactant protein SP-B, Science 261 (1993) 453–456.
[38] M.M. Lipp, K.Y.C. Lee, J.A. Zasadzinski, A.J. Waring, Phase and morphology changes in lipid monolayers induced by SP-B protein and its amino-terminal peptide, Science 273 (1996) 1196–1199.
[39] M.M. Lipp, K.Y.C. Lee, J.A. Zasadzinski, A.J. Waring, Phase and morphology changes in lipid monolayers induced by SP-B protein and its amino-terminal peptide, Science 273 (1996) 1196–1199.
[40] M.M. Lipp, K.Y.C. Lee, D.Y. Takamoto, J.A.N. Zasadzinski, A.J. Waring, Coexistence of buckled and flat monolayers, Phys. Rev. Lett. 81 (1998) 1650–1653.
[41] E.J.A. Veldhuizen, A.J. Waring, F.J. Walther, J.J. Batenburg, L.M.G. van Golde, H.P. Haagsman, Dimeric N-terminal segment of human surfactant protein B ($dSP\text{-}B_{1-25}$) has enhanced surface properties compared to monomeric $SP\text{-}B_{1-25}$, Biophys. J. 79 (2000) 377–384.
[42] R.V. Diemel, M.M.E. Snel, A.J. Waring, F.J. Walther, L.M.G. van Golde, G. Putz, H.P. Haagsman, J.J. Batenburg, Multilayer formation upon compression of surfactant monolayers depends on protein concentration as well as lipid composition: an atomic force microscopy study, J. Biol. Chem. 277 (2002) 21179–21188.
[43] J. Ding, I. Doudevski, H.E. Warriner, T. Alig, J.A.N. Zasadzinski, A.J. Waring, M.A. Sherman, Nanostructure changes in lung surfactant monolayers induced by interactions between palmitoyloleoylphosphatidylglycerol and surfactant protein B, Langmuir 19 (2003) 1539–1550.
[44] R. Mendelsohn, J.W. Brauner, A. Gericke, External infrared reflection-absorption spectrometry. Monolayer films at the air-water interface, Annu. Rev. Phys. Chem. 46 (1995) 305–334.
[45] R.A. Dluhy, Infrared spectroscopy of biophysical monomolecular films at interfaces: theory and applications, Appl. Spectrosc. Rev. 35 (2000) 315–351.
[46] R.A. Dluhy, K.E. Reilly, R.D. Hunt, M.L. Mitchell, A.J. Mautone, R. Mendelsohn, Infrared spectroscopic investigations of pulmonary surfactant. Surface film transitions at the air-water interface and bulk phase thermotropism, Biophys. J. 56 (1989) 1173–1181.
[47] B. Pastrana-Rios, S. Taneva, K.M.W. Keough, A.J. Mautone, R. Mendelsohn, External reflection absorption infrared spectroscopy study of lung surfactant proteins SP-B and SP-C in phospholipid monolayers at the air/water interface, Biophys. J. 69 (1995) 2531–2540.
[48] A. Gericke, C.R. Flach, R. Mendelsohn, Structure and orientation of lung surfactant SP-C and L-α-dipalmitoylphosphatidylcholine in aqueous monolayers, Biophys. J. 73 (1997) 492–499.
[49] C.R. Flach, A. Gericke, K.M.W. Keough, R. Mendelsohn, Palmitoylation of lung surfactant protein SP-C alters surface thermodynamics, but not protein secondary structure or orientation in 1,2-dipalmitoylphosphatidylcholine Langmuir films, Biochim. Biophys. Acta 1416 (1999) 11–20.
[50] F. Ismoyo, Y. Wang, A.A. Ismail, Examination of the effect of heating on the secondary structure of avidin and avidin-biotin complex by resolution-enhanced two-dimensional infrared correlation spectroscopy, Appl. Spectrosc. 54 (2000) 939–947.
[51] C.P. Schultz, O. Barzu, H.H. Mantsch, Two-dimensional infrared correlation analysis of protein unfolding: use of spectral simulations to validate structural changes during thermal denaturation of bacterial CMP kinases, Appl. Spectrosc. 54 (2000) 931–938.
[52] M.-J. Paquet, M. Laviolette, M. Pezolet, M. Auger, Two-dimensional infrared correlation spectroscopy study of the aggregation of cytochrome c in the presence of dimyristoylphosphatidylglycerol, Biophys. J. 81 (2001) 305–312.